Soft Matter

Accepted Manuscript

This article can be cited before page numbers have been issued, to do this please use: M. Li, M. Hosseinzadeh, I. Pagonabarraga, R. Seemann, M. Brinkmann and J. B. Fleury, *Soft Matter*, 2020, DOI: 10.1039/D0SM00460J.

ROYAL SOCIETY OF CHEMISTRY

rsc.li/soft-matter-journal

View Article Online
DOI: 10.1039/D0SM00460J

Soft Matter

ARTICLE TYPE

Cite this: DOI: 00.0000/xxxxxxxxxx

Kinetics of Active Water/Ethanol Janus Droplets

Menglin Li,[a] Mahmoud Hosseinzadeh,[a] Ignacio Pagonabarraga,[b] Ralf Seemann,[a] Martin Brinkmann,[a,c] and Jean-Baptiste Fleury,*[a]

Received Date
Accepted Date

DOI: 00.0000/xxxxxxxxxx

Droplets made of a water/ethanol mixture spontaneously self-propel in an oil/surfactant solution and, depending on the initial ethanol concentration at the time of production, may evolve in up to three stages. Upon self-propulsion the droplets absorb surfactant molecules during their continuous motion in the oily phase. In combination with the continuous loss of ethanol this mass exchange with the ambient phase may lead to a spontaneous phase separation of the water/ethanol mixture, and eventually to the formation of characteristic Janus droplets. Supported by experimental evidence, we propose a simple model that is able to explain the propulsion velocity and its scaling with the droplet radius in the last stage of the droplet evolution.

1 Introduction

Self-propulsion is the ability of objects to continuously move through an ambient liquid in the absence of external forces acting on them[1–3]. In recent years, a growing number of studies have been dedicated to the production of self–propelled liquid droplets. These works were motivated not only by potential applications in biochemical engineering but also by the need for a larger class of model systems to study the collective dynamics of active objects. A number of physical mechanisms linked to chemical reactions, torques on magnetic beads, or gradients of laser light intensity can be exploited to create directed flows around liquid droplets that lead to self–propulsion[1,4–11].

The by far most prominent propulsion mechanism of droplets are Marangoni flows which are driven by surface tension gradients on the liquid-fluid interfaces. These gradients can be sustained by chemical reactions[12], solubilization[13–15], liquid–liquid phase separations[16,17], or by a diffusion-advection controlled reaction of surfactant mixtures at the droplet interface[1]. Not only the realization of active droplets has been proven difficult[18–22] but also the formulation of a consistent physical model that explains self-propulsion by Marangoni flows is a demanding task[15,19].

Self-propelling droplets of initially pure water/ethanol droplets in an oily solution of monoolein were recently proposed as programmable smart carriers for biological material[15]. Here we present the results of a systematic experimental study of the droplet system reported in[15] with the aim to quantify the evolution and to find evidence for potential driving mechanisms that control the velocity of their motion. Based on the experimental data we propose a simple model for self-propulsion that explains relevant features related to the evolution of the propulsion velocity.

It has been conjectured in Ref.[15] that the self-propulsion is the consequence of a continuous release of ethanol from the droplet into the oil phase and a simultaneous uptake of monoolein. This hypothesis is supported by the observation that the droplets spontaneously separate into a water-rich droplet and a droplet of an monoolein-rich ethanol phase a certain time after production. The formation of these Janus droplet varies between seconds to several minutes or may be even absent at high ethanol concentrations[15].

To explain the kinetics and morphological evolution of the droplets we propose a simple model explaining the motion from the chemical disequilibrium of monoolein which acts as a 'fuel'. While the exchange of substances of the droplet phase with the surrounding phase cannot be quantified in our experiments, we are able to model the associated propulsion mechanism and predict the duration and velocity in certain phases of the evolution and, hence, to *program* micro-droplets to perform certain tasks as demonstrated in Ref.[15].

2 Material

Observation chambers were fabricated from glass slides cut into squares of about (2.5×2.5) cm^2. These glass squares were precleaned by sonication in ethanol, acetone and toluene for 10 min each, and blow-dried with nitrogen gas after each cleaning step. After pre-cleaning, the squares were immersed for 30 min in Piranha etch (50 vol.% sulfuric acid (98 vol.%) and 50 vol.% hy-

[a] Experimental Physics, Saarland University, 66123 Saarbrücken, Germany, E-mail: jean-babtiste.fleury@physik.uni-saarland.de
[b] Department of Condensed Matter Physics, University of Barcelona, Carrer de Marti i Franques 1, Barcelona, Spain
[c] Smart Materials & Surfaces Laboratory, Faculty of Engineering & Environment, Northumbria University, Newcastle upon Tyne NE1 8ST, UK

† Electronic Supplementary Information (ESI) available: [details of any supplementary information available should be included here]. See DOI: 10.1039/b000000x/

View Article Online
DOI: 10.1039/D0SM00460J

drogen peroxide (30 vol.%), and thoroughly rinsed with hot (80–90)°C ultra pure water. Subsequently, the glass squares were immersed in hot water for another 15 min and then again blow-dried with nitrogen. Following this cleaning proceedure, the glass squares were coated with octadecyl-trichlorosilane (OTS). To this end, the glass squares were immersed for 12 min in a solution consisting of 50 ml bicyclohexane, 20–40 drops of carbon tetrachloride, and 5–20 drops of OTS[23,24]. Residual OTS solution was removed from the OTS-coated glass by rinsing it with chloroform followed by blow-drying with nitrogen. Observation chambers were finally made out of two OTS coated glass squares with a cover slide (thickness 150 μm) in between. The OTS coated glass squares and the spacers were glued together with epoxy glue. After cross linking of the epoxy glue the cover slide was removed providing the space for the observation chamber.

All chemicals were purchased from Sigma-Aldrich, except the fluorescent lipid (1,2-dipalmitoyl-sn-glycero-3-phosphoethanolamine- N-7-nitro-2-1,3-benzooxadiazol-4-yl; CAS Number: 810144P), which was purchased from Avanti Polar Lipids.

At the beginning of each experiment droplets of a homogeneous water/ethanol mixture are ejected into squalane from the tip of a micro-pipette. If not mentioned otherwise, the squalane contains the surface active substance monoolein at a concentration of 10 mM. This concentration is well above the critical micellar concentration (CMC) and we thus assume that the majority of monoolein molecules are present in the form of micelles. Squalane and water are almost immiscible but squalane dissolves 4 vol.% of ethanol at room temperature[15].

3 Results

A certain time after production, the initially spherical and homogeneous droplets of the ethanol/water mixture undergo a bulk phase separation and may form compound droplets consisting of two liquid phases that are both immiscible with the surrounding squalane phase.

The stages of the evolution, and the duration to the onset of the phase separation is controlled by the ethanol concentration in the droplet at the time of production. We will first discuss the observations for an medium ethanol concentration and continue later with the qualitative and quantitative differences at lower or higher initial ethanol concentrations.

Medium ethanol concentrations: For initial ethanol concentrations ranging from about 40 vol.% to approximately 70 vol.%, the majority of droplets start to self-propel in the oily phase immediately after production. During this stage 1 the droplets remain spherical and optically homogeneous, cf. Fig. 1. During self-propulsion in stage 1 every droplet looses a few percent of its volume, and takes up monoolein molecules from the surrounding phase. This volume loss is higher for droplets with a higher initial ethanol concentration.

The influx of monoolein to the moving droplet is monitored by adding the fluorescent lipid dye 1,2-dipalmitoyl-sn-glycero-3-phosphoethanolamine- N-7-nitro-2-1,3-benzooxadiazol-4-yl to the initially pure water/ethanol mixture, cf. the fluorescent microscopy image Fig. 1. Similar to monoolein, the fluorescent lipid dye displays a strong affinity to ethanol and follows the repartition of monoolein molecules between the fluid phases.

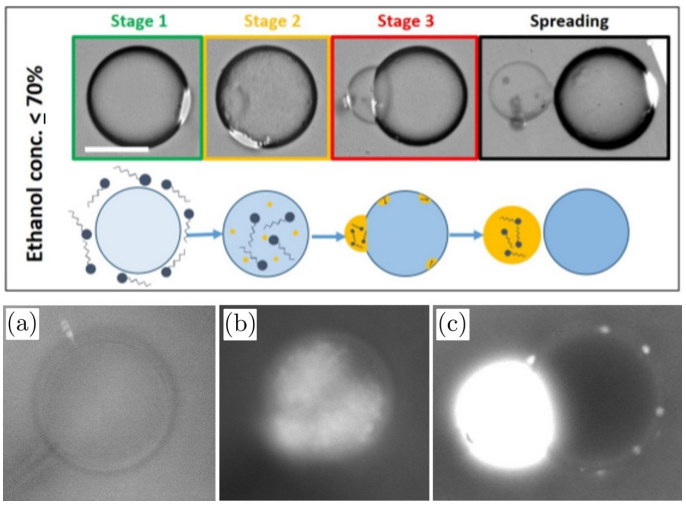

Fig. 1 Upper Panel: Evolution stages of self-propelled droplets with an initial ethanol concentration in the range of $40-70$ vol.%. Top row: Optical micrographs. Bottom row: sketches of the droplets, where the intensity of the blue and yellow colors indicate increasing concentration of water and ethanol respectively. The white scale bar in the optical images represents $100\,\mu$m. Lower Panel: Fluorescent microscopy image self-propelling droplets in fluorescent microscopy. (a) Droplet in stage 1 with an initial ethanol concentration of 60 vol.% displaying plumes and a dark wake. (b) Nucleation of small ethanol-rich minority droplets inside the mother droplet. (c) Janus droplet in stage 3 with an initial ethanol concentration of 50 vol.% displaying the nucleation and growth of small droplets of ethanol-rich phase on the surface of the leading water-rich droplet.

The fluorescent lipid dye dispersed in the oily phase also reveals a wake behind the droplet, cf. Fig. 1 (a), which is indicative of a thin depletion layer around the self-propelling droplet. Finally, after 1-3 minutes a phase separation occurs in the bulk of the droplets, marking the end of stage 1. Figure 1 displays a droplet in the beginning of the following stage 2. Apparently, the entire droplet appears blurry in transmission microscopy because of the enhanced scattering of light at the fluctuations of the composition at the onset of phase separation. Only a few seconds after the beginning of stage 2, small droplets of a minority phase become visible. These droplets are rich in monoolein and ethanol as indicated by the enrichment of fluorescent lipid dye in the minority phase, cf. Fig1 (b).

The nucleation of ethanol and monoolein-rich small droplets inside the bulk of the 'mother droplet' lasts for about 1-2 minutes. In the course of stage 2, the initially small ethanol and monoolein-rich droplets coalesce and coarsen into a single large droplet, cf. the fluorescent microscopy image in Fig. 1. The latter droplet is found in the rear of the moving water-rich droplet. Finally the ethanol-rich droplet is pushed out and trails behind the leading water-rich droplet. At this point, the nucleation in the bulk ceases and the initially spherical and homogeneous droplet has transformed into a Janus droplet illustrated in Fig. 1. This characteristic shape transformation marks the end of stage 2.

In the following stage 3 these Janus droplets self-propel for about $5-10$ min. Close inspection of the leading droplet in Fig. 1

View Article Online
DOI: 10.1039/D0SM00460J

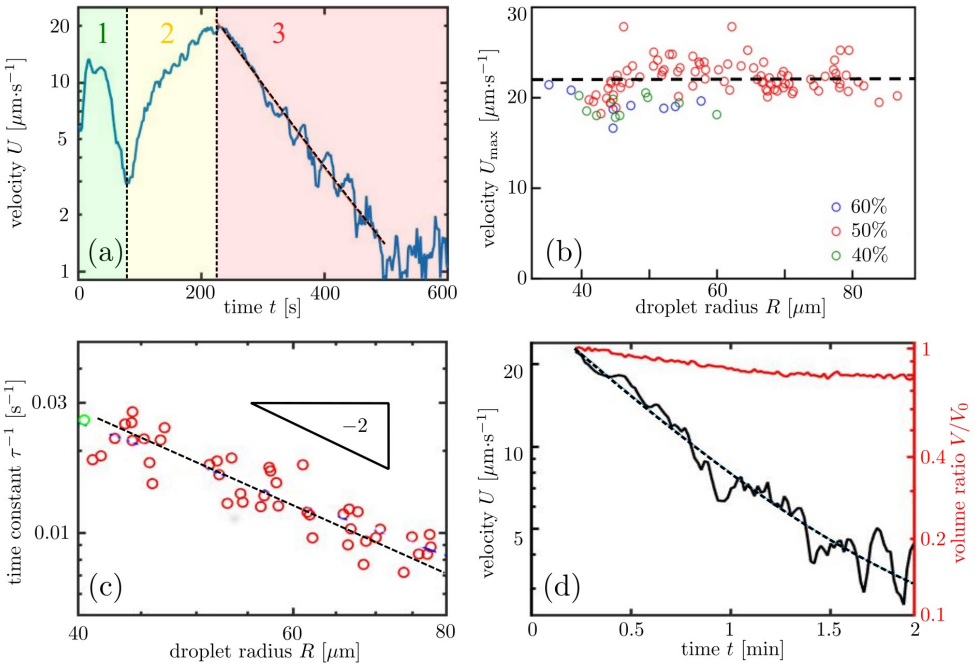

Fig. 2 (a): Velocity evolution of a self–propelling droplet with an initial ethanol concentration of 50 vol.% and an initial radius of 40 μm. The dashed line illustrates the exponential fit of the velocity decay in stage 3 according to Eq. (15) which yields a time constant $\tau^{-1} = 0.027\text{s}^{-1}$. (b): Maximum velocity U_{max} of self-propelling droplets in stage 2 plotted against the droplet radius R, for initial ethanol concentration of 40%, 50%, 60%. The dashed line indicates the average of U_{max} over the entire data set.(c): Scaling of the time constant τ of the exponential velocity relaxation in stage with the droplet radius R for an initial ethanol concentration of 50 vol%.(d):Velocity U of a self-propelling Janus droplet in stage 3 in comparison to the ratio of the actual volume V of the leading droplet to the initial volume V_0 at the end of stage 2 as a function of time t. The datum of the green symbol in (c) corresponds to the droplet analyzed in (a).

reveals the nucleation of tiny ethanol-rich droplets. In contrast to the formation of ethanol-rich minority phase droplets in the bulk of the mother droplet in stage 2, these small ethanol-rich droplets appear and grow on the interface between the leading droplet and the ambient oil phase (clearly visible in supplementary movie 3). These tiny droplets are quickly advected by the swirling flow toward the rear of the leading droplet where they finally coalesce with the trailing (ethanol-rich) droplet. As a consequence of this process, the volume of the leading droplet in stage 3 decreases while the volume of the trailing droplet increases.

The appearance and growth of the tiny droplets also influences the trajectories of active Janus droplets. Droplets moves persistently into the same direction if there are nearly equal numbers of these tiny droplets on either sides of the surface of the leading droplet, cf. Fig. 3. However, if there is an imbalance in the density of tiny droplets, the leading edge of the Janus droplet turns into the direction of the side that is decorated with the smaller number of tiny droplets, cf. Fig. 3.b. Therefore, the trajectories of active droplets could be predicted knowing the distribution of tiny droplets on the surface of the leading water-rich droplet.

At the end of stage 3, the two droplets forming the compound Janus droplet may break up, as illustrated in Fig. 1. After separation of the ethanol- and monoolein-rich trailing droplet from the leading droplet, the former typically spreads on the hydrophobic substrate upon touching. In the majority of cases, the motion of the water-rich and monoolein-poor leading droplet stops immediately after separation. In rare cases, however, the leading droplet continues to self-propel by a few droplet radii.

During all evolution stages, the overwhelming majority of droplets with an initial ethanol concentration of 50 vol.% are continuously self-propelling. Droplets that are not moving immediately after their production do not start to self-propel until the end of the experiment. Also the magnitude of the self-propulsion velocity may vary pronounced between each stage and between droplets in the same stage but with different initial ethanol concentrations.

In stage 1 the ethanol/water droplets self-propel at a constant velocity after a few seconds, albeit with strong fluctuations. Towards the end of stage 1, a decrease of the self-propelling velocity is observed, cf. the example for the velocity evolution shown in Fig. 2(a). The minimum velocity is reached at the transition between stage 1 and 2. The value of the velocity in this minimum scatters strongly and a systematic dependence on the initial droplet radius could not be observed in our experiments.

In the following stage 2, the self-propelling droplet accelerates until a maximum velocity is reached, cf. Fig. 2(a). The value of the maximum velocity is independent on the droplet radius in the range between 40 μm and 90 μm considered in this work, cf. the plot of U_{max} against R in Fig. 2(b).

A typical velocity evolution of a droplet in stage 3 with an initial ethanol concentration of 50 vol.% is shown in Fig. 2 (a) in comparison to a fit with an exponential decay of the form

$$U(t) = U_{max} e^{-t/\tau} + U_\infty \,. \qquad (1)$$

View Article Online
DOI: 10.1039/D0SM00460J

allowing a plateau of constant velocity $U_\infty \ll U_{\max}$ at large times.

Exponential fits of the from (1) to the measured velocity evolution for a large number of droplets reveal that the maximum $U_{\max}$ does not depend on the droplet size, cf. Fig 2(b). At large times, the velocity of the Janus droplet in stage 3 fluctuates around a small cruising velocity $U_\infty \ll U_{\max}$ and once the velocity has fallen below a value $\approx 1-2\mu$m/s, the droplet starts to interact with the substrates until, eventually, becomes pinned.

The double logarithmic plot Fig. 2(c) of the decay time τ of the fits not only illustrates that τ increases with the initial droplet radius R but also reveals a clear power law scaling $\tau \propto R^\alpha$ with an exponent of $\alpha = 1.6 \pm 0.3$. A correlation of the velocity decay in stage 3 with the volume decay of the leading droplet can be observed in Fig. 2(d). In this example, the relative volume loss of the leading droplet is $(V_0 - V_\infty)/V_0 \approx 0.2$ while the velocity ratio is $U_\infty/U_{\max} \approx 0.05$.

Low initial ethanol concentration: In droplets with a low initial ethanol concentration of about 30 vol.%, or lower, the demixing starts almost immediately after the droplet is placed in the squalane. At these low initial ethanol concentration the droplets directly begin to self-propel in stage 2, in contrast to the case of droplets with a medium initial ethanol concentration. Also duration of demixing in stage 2 is shorter than the one for a droplet with medium initial ethanol concentrations. Self-propulsion of the formed Janus droplets in stage 3 can effectively be observed only for around 5 min. Qualitatively, stages 2 and 3 for low ethanol concentration are identical to the evolution stages for droplets with a medium initial ethanol concentration described above. Reducing the initial ethanol concentration in the droplets even below 30 vol.%, phase separation is not always observed and self-propelled motion is not occurring reliably.

High ethanol concentration: Droplets with an initial ethanol concentration between ≈ 70 vol.% to ≈ 80 vol.% display all three evolution stages as shown in Fig. 4. Stage 1 extends to $10-15$ min before the phase separation at the beginning of stage 2. In addition to the boundary layer, we observe microscopic dark clouds or plumes at the surface of active droplet during self-propulsion in stage 1. The spatial extension of the plumes in the ambient phase is the larger the higher the initial ethanol concentration. Moreover, for the range of tested water/ethanol ratios, the spatial extension is decreasing with time during the self-propulsion in stage 1.

The duration of the subsequent de-mixing in stage 2 lasts for around $1-2$ min. In contrast to the intermediate and low ethanol concentrations, the water-rich phase is now the minority phase and several water-rich droplets are formed inside the ethanol-rich droplet. Accordingly, the water-rich droplets are finally pushed out of the larger ethanol-rich droplet and may continue to locomote. The ethanol-rich mother droplet spreads on the OTS-coated bottom of the device and thus stops moving. Production of droplets with ethanol concentrations well above 80 vol.% is not possible as those droplets directly spread on the OTS-coated bottom of the observation chamber.

4 Model

Predictive models to quantify the factors that control the duration and velocity of a self-propelling droplet are useful in a variety of applications[15]. In the following we propose a simple model that explains the velocity of self-propulsion in the different stages of their evolution as well as the time between droplet production and phase separation from a mass exchange between the fluid phases.

Any motion of the self-propelling droplets considered in this work is driven by surface tension gradients on the interface between the water/ethanol/monoolein mixture and monoolein dissolved in squalane as ambient fluid. These surface tension gradients are caused by spatial variations in the local composition of the fluid mixtures. Spontaneous self-propulsion of the droplet persists as long as a chemical non-equilibrium of the components in the droplet and ambient fluid phase is maintained. Hence, the self-propulsion must vanish once a chemical equilibrium of all components is reached.

A number of possible mechanisms can explain the self-sustained interfacial tension gradient on the surface of self-propelling droplet in stage 1. These mechanisms have in common that they rely on diffusive transport of monoolein molecules in the squalane phase to the droplet surface and on a concomitant diffusion of ethanol from the droplet surface into the ambient squalane phase. Here, it is reasonable to assume that the diffusion of monoolein micelles in the squalane phase to the droplet surface is the slowest process in the chemical equilibration process and, thus, chiefly controls the surface tension gradients. For the sake of simplicity, solutal Marangoni stresses due to ethanol concentration gradients in the coexisting phases at droplet surface will be neglected.

4.1 Stage 1

It is instructive to consider the situation where the droplet and the ambient squalane phase are at rest. By this assumption any mass transport by advection is ruled out. Chemical equilibration is controlled by the diffusive flux and the concentration profiles of all components as well as the gradients in the local chemical composition of the phases are spherically symmetric.

This quiescent droplet state can now be stable or unstable against small displacements of the droplet's center of mass. If a droplet is in chemical equilibrium with the ambient phase before the displacement, the surface coverage Γ of monoolein molecules in response to the displacement and surface coverage should decrease in front of the droplet and increase in the rear due to surfactant being swept backward. Since $\partial\gamma/\partial\Gamma < 0$ for a surface active substance like monoolein, an opposing gradient in the surface tension builds up in response to a small displacement and the droplet is pushed back into its original position. A sustained self-propulsion in the direction of the displacement is observed only if the surface coverage in the rear of the droplet is actively kept at a lower value than in the front.

Surface coverage gradients that propel the droplet may occur if, in addition to a quick repartition of monoolein between squalane and the ethanol/water mixture, the diffusion of the monoolein

View Article Online
DOI: 10.1039/D0SM00460J

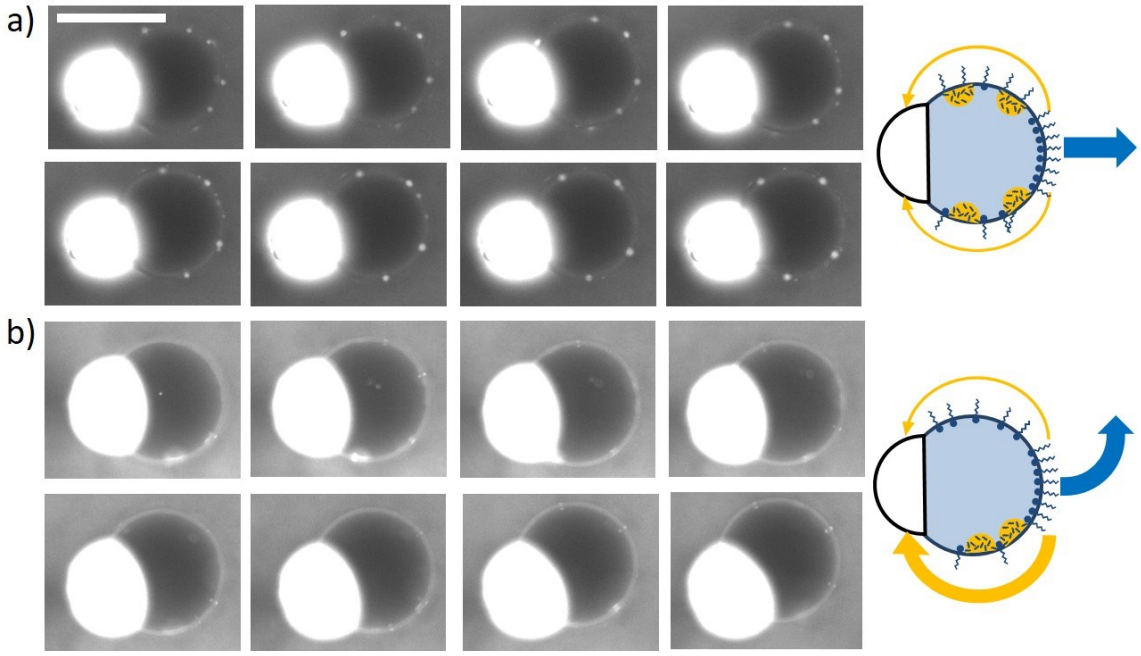

Fig. 3 Fluorescent microscopy image of self-propelling droplets. Scale bar is $100\,\mu$m for all images. a) Optical micrographs of a self-propelling droplet in a relatively straight motion. b) Optical micrographs of a rotating self-propelling droplet. Sketches of a droplet motion depending of a the density of the secondary droplet nucleation (presented in yellow). In both panels the time frame between two consecutive frames is ≈ 0.3s .

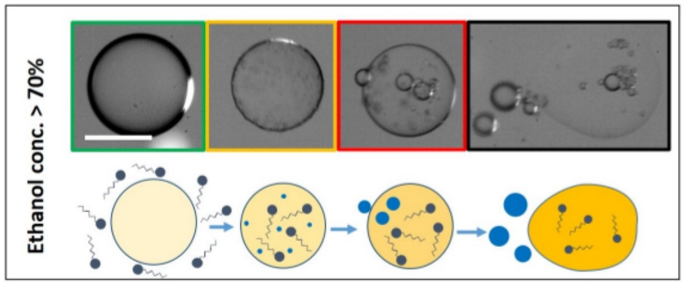

Fig. 4 Evolution stages of self-propelled droplets with an initial ethanol concentrations > 70vol.%. Top row: Optical micrographs. Bottom row: sketches of the droplets, where the intensity of the blue and yellow colors indicate increasing concentration of water and ethanol, respectively. The white scale bar in the optical image is $100\,\mu$m.

in ethanol/water is much faster compared to the diffusion in squalane. In this case, a monoolein depleted layer forms around the droplet immediately after production. Because of the high solubility of monoolein in ethanol it is reasonable to assume that the monoolein concentration c_0 at the surface of the droplet is much smaller than the monoolein concentration c_∞ in the squalane far away from the droplet. Using $c_0/c_\infty \approx 0$ we can estimate the concentration gradient on the surface to be $\nabla c \approx c_\infty/\delta$ where δ denotes the extension of the monoolein depleted layer. As the monoolein molecules quickly dissolve into the bulk of the ethanol/water phase we assume a quasi-steady dynamic equilibrium $j_a = j_d$ of the diffusive current $j_a = D\nabla c$ and the dissolution rate per area, $j_d = k\Gamma$. The kinetic constant k controls the number of monoolein molecules dissolving from the surface into the ethanol–rich phase per unit time. Using the estimate of the concentration gradient, we arrive at the relation $\Gamma \approx k^{-1}c_\infty/\delta$ stating that the surface coverage of monoolein will be the higher the lower the thickness of the boundary layer.

A displacement of an initially quiescent droplet will now lead to smaller thickness of the depletion layer in the direction of the displacement and to an increase of the thickness at the opposite side of the droplet. Because the monoolein coverage on the adsorbing droplet surface is the larger the thinner the boundary layer, we will now observe a surface tension gradient with opposite sign which drives the droplet further into the direction of the initial displacement.

The idea of a monoolein depleted diffusive boundary layer in the oil phase whose thickness grows while the oil flows past the droplet can also be used to estimate the average thickness $\langle\delta\rangle$ of the boundary layer of a moving droplet. Assuming $\delta = 0$ and an infinite gradient at the time of production $t = 0$, the thickness δ of the depletion layer will first grow as $\delta \approx \sqrt{D\,t}$. Considering a self-propelled droplet moving with a constant velocity U, we can argue that the average value of the thickness will quickly saturate to $\langle\delta\rangle \approx \sqrt{D\,t_c} = R/\sqrt{\mathrm{Pe}}$ where $t_c = R/U$ is the convective time scale of the flow. The Peclet number $\mathrm{Pe} = RU/D$ of the steadily self-propelling droplets can be computed from the propulsion velocity U, the droplet radius R, and the diffusion constant D of monoolein micelles in the squalane phase. Following the Stokes-Einstein relation $D = k_bT/6\pi\eta_o r_h$ with a temperature of $T = 300$K,a dynamic viscosity of squalane $\eta_o = 3.0\cdot 10^{-2}$Pa·s, and a hydrodynamic radius $r_h = 2$nm for the micelles, we arrive at a diffusion constant $D = 3.7\cdot 10^{-12}\,\mathrm{m}^2/\mathrm{s}$ of the monoolein micelles. For a typical velocity $U = 10\,\mu$m/s, and a droplet radius $R = 50\,\mu$m we have $\mathrm{Pe} \approx 140$ and a thickness–to–radius ratio of the boundary layer $\delta/R \approx 1/\sqrt{\mathrm{Pe}} \approx 0.083$. From estimates of the core diameter of the dark trail, (or wake) we conclude that the

View Article Online
DOI: 10.1039/D0SM00460J

thickness of the boundary layer remains small compared to the radius of the self-propelling droplet. In stage 1 and 2, the depletion layer could be estimated from the thickness of the black trail behind the self-propelling droplet. In stage 3, this estimate could not be performed because the trailing ethanol droplet absorbs all the fluorescent molecules along the motion of the active Janus droplet. Thus, it shields the fluorescent estimation of our monoolein-depleted boundary layer.

The idea of a monoolein depleted boundary layer around the swimming active droplet can be also employed to estimate the total number of monoolein molecules adsorbed in stage 1 within time t:

$$N \approx 4\pi R^2 \langle j_a \rangle t \approx 4\pi \sqrt{DUR^3}\, c_\infty t \ . \tag{2}$$

Using the number of monoolein molecules in the droplet at the onset of phase separation $N^* = 4\pi R^3 c^*/3$, where c^* denotes the monoolein concentration in the droplet at the onset of phase separation, we arrive at the estimate

$$t^* \approx \frac{1}{3}\sqrt{\frac{R^3}{DU}}\frac{c^*}{c_\infty} \ . \tag{3}$$

for the duration of stage 1 which is, apart from the prefactor, identical to the expression proposed in Ref.[15].

4.2 Stage 2

Modeling the kinetics of propulsion in the following stages 2 and 3 requires an understanding of the equilibrium phase behavior of the components, in particular, the shape of the-two phase region in the equilibrium phase diagram of the ternary mixture of monoolein, water, and ethanol. Based on the observation that squalane is virtually insoluble in a water/ethanol mixtures, we can restrict our consideration to ternary mixtures of water/ethanol/monoolein. Semi-quantitative ternary phase diagrams displaying boundaries between single and two-phase regions, and a few complex micro-phases at high monoolein concentrations are described in Refs.[26,27]. A tentative form of the phase diagram of the ternary mixture ethanol/water/monoolein summarizing the findings in Refs.[26,27] is shown in Fig. 5.

A prolonged delay of the phase separation in the self-propelling droplets observed for higher initial ethanol concentration agrees with the assumption that the droplet looses more ethanol and takes up more monoolein from the surrounding squalane phase to reach the two-phase region of the water/ethanol/monoolein phase diagram[26–28] shown in Fig. 5. Once the amount of adsorbed monoolein has reached a certain threshold value, the bulk of the initially homogeneous droplet spontaneously de-mixes into an ethanol-rich and a water-rich liquid phase.

The temporal evolution of the chemical composition of the active droplet is sketched in Fig. 5 for low and high initial ethanol concentrations. A spontaneous phase separation of the water-/ethanol/monoolein mixture sets in once the chemical compositions crosses the spinodal line in the phase diagram shown as dashed-dotted lines in Fig. 5. At the onset of phase separation, the trajectory splits into two separate curves which closely follow the tie lines until the boundary of the two-phase region is reached. Depending on the position of the crossing point relative

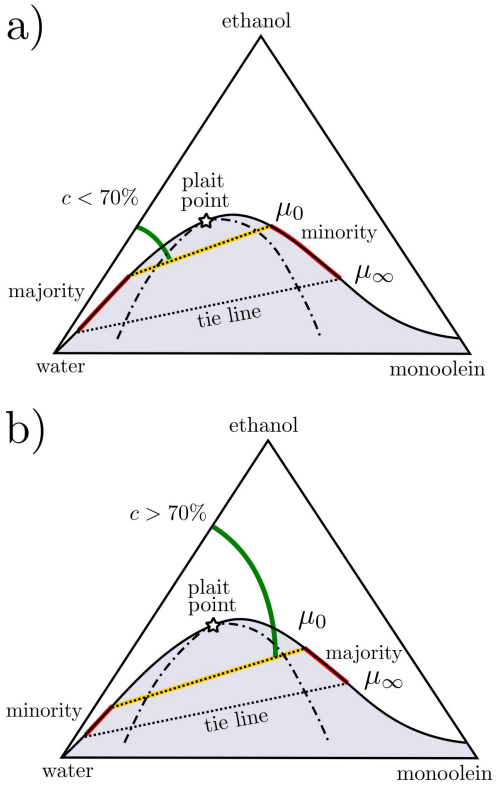

Fig. 5 Sketch of the ternary phase diagram for monoolein/water/ethanol indicating the region of two-phase coexistence (grey) and the spinodal line (dashed-dotted line). Possible trajectories of the composition of the self-propelling droplet for an initial ethanol concentration below and above 70%vol are shown in a) and b), respectively, where the color corresponds to stage 1 (green), stage 2 (orange) and stage 3 (red).

View Article Online
DOI: 10.1039/D0SM00460J

to the plait point, the majority phase may either be ethanol- and monoolein-rich phase Fig.5a) or the water-rich and monoolein-poor phase, cf. Fig. 5 (a) and (b), respectively. Assuming a slow uptake the compositions of the two coexisting phases will be located on the boundary of the two-phase region and connected by a tie line at any time.

4.3 Stage 3

A stable coexistence of the two phases is attained once the composition of both phases have reached the binodal line bounding the two-phase region. After this point, marking the beginning of phase 3, a further decrease of the ethanol concentration in the water-rich phase is achieved by further monoolein entering the Janus droplet. Hence, the compositions of the two coexisting phases follow points on the binodal line corresponding to a common tie line while the demixing degree of ethanol and water in the Janus droplet is controlled by the amount of monoolein that has been taken up from the ambient squalane phase.

With the aim to model the motion of Janus droplets in stage 3, we consider the temporal evolution of the concentration of monoolein molecules $n_t = N_t/V$ in the trailing droplet, where N_t is the number of monoolein molecules and V the volume of the trailing droplet. The rate of change of the monoolein concentration is then

$$\dot{n}_t = \frac{\dot{N}_t}{V} - \frac{N_t \dot{V}}{V^2} \,, \tag{4}$$

where we use the dot as an abbreviation for a time derivative.

The total flux $\dot{N}_t$ of monoolein molecules into the trailing droplet is controlled by two processes. First, small droplets of the freshly nucleated minority phase floating on the surface of the leading droplet in stage 3 coalesce with the trailing droplet and thereby increase the number of monoolein molecules at a rate $\dot{N}_a$, cf. Fig. 1 (c). Second, monoolein molecules adsorbed on the surface of the leading droplet are advected to the three phase contact line and enter the trailing droplet at a rate $\dot{N}_c$.

The following model for self-propulsion in stage 3 neglects the influx of small droplets and the volume change of both the trailing and the leading droplet. Thus, we assume that these tiny droplets do not affect the magnitude of the propulsion velocity.

Using the simplifying assumptions $\dot{N}_a = 0$ and $\dot{V} = 0$, the change of concentration can be simply written as:

$$\dot{n}_t = \frac{N_c}{V} = \frac{2\pi R \langle\Gamma\rangle U}{V} \,, \tag{5}$$

where R is the radius of the leading droplet, $\langle\Gamma\rangle$ the surface coverage of monoolein molecules on the interface between the water-rich phase and the ambient squalane phase, and U the velocity of the self-propelling compound droplet.

To describe the equilibration dynamics it is useful to define the dimensionless undersaturation

$$X \equiv \frac{n_\infty - n_t}{n_\infty - n_0} \tag{6}$$

of monoolein molecules in the trailing droplet, where n_0 and n_∞ are the concentration n_t at $t = 0$ and for $t \to \infty$. Using the definition (6) we can express the rate of change (5) in terms of the change

$$\dot{X} = -\frac{2\pi R \langle\Gamma\rangle U}{(n_\infty - n_0) V} \tag{7}$$

of the dimensionless undersaturation.

One way to obtain the velocity U of self-propulsion in Eqn. (7) is to balance ~~of~~ the injected power released by the monoolein molecules and the power of work dissipated in viscous flows. The power dissipated in the viscous flows is given by

$$\mathscr{P}_{\rm diss} = 6\pi C \eta_o R U^2 \tag{8}$$

where η_o is the dynamic viscosity of the oil phase. The numerical prefactor C depends on the geometry and the ratio of the viscosities of the droplet phase to the ambient squalane phase.

The power injected to the Janus droplet through the uptake of monoolein collected from the interface of the water-rich leading droplet can be written as

$$\mathscr{P}_{\rm inj} = (\mu_\infty - \mu_t)\dot{N}_c = 2\pi (\mu_\infty - \mu_t) R \langle\Gamma\rangle U \,, \tag{9}$$

where μ_t is the chemical potential of monoolein molecules in the trailing droplet. Starting from the balance $\mathscr{P}_{diss} = \mathscr{P}_{inj}$, we obtain the droplet propulsion velocity

$$U = \frac{(\mu_\infty - \mu_t)\langle\Gamma\rangle}{3C\eta_o} \tag{10}$$

which is independent on the droplet radius R. Besides a prefactor, the same expression for maximum propulsion velocity can be obtained from a balance of the Marangoni stress acting on the droplet's surface and the dissipation in viscous flows.

To describe the velocity relaxation in stage 3, we employ a linear expansion of the chemical potential difference:

$$\mu_\infty - \mu_t = \left.\frac{\partial\mu}{\partial n}\right|_{n=n_\infty} (n_\infty - n) + \mathscr{O}\left\{(n_\infty - n)^2\right\} \tag{11}$$

and rewrite Eq. (7) in the form

$$\dot{X} = -\frac{2\pi R \langle\Gamma\rangle^2}{3C\eta_o V} \left.\frac{\partial\mu}{\partial n}\right|_{n=n_\infty} X \,. \tag{12}$$

Owing to the linear approximation in our model, the propulsion velocity $U(t)$ of the Janus droplet is strictly proportional to the non-dimensional monoolein undersaturation $X(t)$ in the trailing droplet:

$$U(t) = U_{\rm max} X(t) \,. \tag{13}$$

Hence, the maximum velocity $U_{\rm max}$ is attained for the maximum possible difference of chemical potential on the droplet surface:

$$U_{\rm max} = \frac{(n_\infty - n_0)\langle\Gamma\rangle}{3C\eta_o} \left.\frac{\partial\mu}{\partial n}\right|_{n=n_\infty} \,. \tag{14}$$

The solution of the differential equation (12) in time t is an exponential decay

$$U(t) = U_{\rm max}\, e^{-t/\tau} \tag{15}$$

View Article Online
DOI: 10.1039/D0SM00460J

with a time constant

$$\tau^{-1} = \frac{2\pi R \langle \Gamma \rangle^2}{3C\eta_o V} \left. \frac{\partial \mu}{\partial n} \right|_{n=n_\infty} \quad (16)$$

For droplets with the same initial ethanol concentration at the time of production, the volume V of the ethanol-rich trailing droplet at the end of stage stage 3 will be proportional to the initial volume of the mother droplet. If we assume a purely advective transport of monoolein into the trailing droplet, the time constant of the velocity relaxation in stage 3, as given by Eq. (16), will scale as $\tau^{-1} \propto R^{-2}$, where R is the initial radius of the mother droplet.

The size independent maximum velocity $U_{\max}$ of the droplets at the beginning of stage 3 is in very good agreement with the experimental data shown in Fig. 2.b. Taking into account the uncertainty of the power law fit, the exponent $\alpha = 1.6 \pm 0.3$ of the scaling $\tau \propto R^\alpha$ (Fig. 2.c) determined from the experimental data is only slightly smaller than the value $\alpha = 2$ predicted by the model.

5 Discussion

The observation of a certain, but small fraction of droplets that do not move after production could be linked to pinning the droplets by impurities on the bottom surface of the cell. Another possible origin for the existence of quiescent droplets could lie in the growth kinetics of the monoolein-depleted boundary layer at the beginning of the experiment. Monoolein-depleted boundary layers whose thickness exceed a certain threshold may not allow sufficient Marangoni stresses to bring the droplet into a continuously self-propelling state. A dynamic bistability between a self-propelling and a quiescent stationary states has already been proposed in Ref.[32]. Their weakly-nonlinear stability analysis is based on a similar diffusion and reaction-controlled model of the surfactant transport but is restricted to asymptotically small Peclet numbers[32].

Simultaneously to the dissolution of monoolein in the droplet, a certain amount of ethanol will dissolve in the ambient squalane phase during self-propulsion. Gradients of ethanol concentration close to the surface of the moving droplet may also contribute to Marangoni stresses in all stages of the evolution. The increasing droplet velocity in the following stage 2 of the droplet evolution can be explained in terms of an increasing magnitude of the derivative $\partial\gamma/\partial\Gamma$ of the surface tension γ between the leading droplet and the ambient oil phase during phase separation. A decreasing ethanol concentration in the majority phase could give rise to higher Marangoni stresses, and thus to faster self-propulsion.

Alternative to the self-sustained surface tension gradients driven by the fast repartition of monoolein molecules from the squalane into the ethanol-rich droplet creating a monoolein depleted layer in the squalane phase, one could explain spontaneous self-propulsion from a swelling of monoolein micelles with ethanol in the vicinity of the droplet's surface. This swelling mechanism has been proposed for nematic liquid crystal droplets that self-propel in an aqueous ionic surfactant solution[33]. In this case, the surfactant molecules desorb from the rear of the droplet during a spontaneous emulsification. The corresponding trail of tiny nematic liquid crystal droplets covered with the surfactant can be clearly observed in optical microscopy[33]. In the present system, however, the swelling mechanism proposed in Ref.[33] is not able to explain the formation of the dark trail left behind the droplet. The high affinity of the lipid dye to the ethanol in the micelles would rather increase the fluorescence intensity in the droplet's wake. The observed reduced intensity, however, is well in line with a dye depleted boundary layer that has separated from the droplet.

But not only the trail, also the dark clouds or plumes observed in the course of stage 1 can be a direct consequence of the monoolein and dye depleted boundary layer in the squalane phase. The gradients in the monoolein surface coverage may give rise to several smaller convection cells at the surface of the droplet instead of a single axially symmetric convection cell driven by Marangoni stresses. These cells advect the monoolein depleted layer close to the droplet into the surrounding bulk phase which become visible as plumes. Advection and separation of the dye depleted boundary layer at a converging stagnation points of the convection cells can easily explain the dark plumes visible in fluorescent microscopy.

Despite its simplicity, the model captures the qualitative behavior of the active Janus droplet motion in stage 3 and is able to predict a radius independent maximum velocity at the beginning of stage 3. The maximum velocity corresponds to the largest difference between the chemical potential of the monoolein molecules in the ambient squalane phase and in the ethanol–rich trailing droplet at the time when the minority phase droplets form a three–phase contact line.

The assumption that the surrounding oil phase is not altered in the presence of the self-propelling droplets might be reasonably well fulfilled only for a single droplet. In the experiments reported here, we prepared typically a group of droplets in one cell which could change the monoolein concentration in the surrounding squalane phase over time. The decrease of available surfactant in the oil phase may not only explain the slight deviation of power law exponent of the relaxation time in terms of the droplet radius but also the non-zero final velocity at the end of stage 3.

Nucleation of tiny ethanol-rich droplets on the surface of the leading droplet affects the trajectories of the self-propelling Janus droplets. Each of the tiny droplets will generate a Marangoni flow convection roll similar the one of the big trailing droplet in the rear of the Janus droplet. If there are a nearly equal numbers of these tiny droplets on either sides of the leading droplet's surface, the resulting stress generated by the tiny droplets cancels out and the Janus droplet keeps a persistent motion (see Fig.3.a). If they are more tiny droplets on one side of the leading droplet, the Marangoni flow around the tiny droplets enhances backward flow on the side with an excess of tiny droplets. As a results the Janus droplets turns to the side with the lower number of tiny droplets and continues to propel into the new direction after the tiny droplets causing the imbalance have coalesced with the trailing droplet (see Fig.3.b)

View Article Online
DOI: 10.1039/D0SM00460J

6 Conclusions

Sponteneous self-proplusion and the evolution of droplets made of a water/ethanol mixture in an oil/surfactant solution can be explained from an absorbtion of surfactant molecules from the oily phase in combination with the continuous loss of ethanol. A simple model based on the assumption of a thin surfactant depleted boundary layer in the oil phase is put forward to explain the duration and propulsion velocity associated to the stages of the droplet evolution. The existence of the thin surfactant depleted boundary layer in the oil phase is evidenced by a dark trail in the wake of the self-propelling droplet. The model presented in this work not only captures the delayed onset of phase separation occuring in the bulk of the droplets, it also explains the exponential velocity relaxation of the Janus droplets in stage 3 as well as the scaling of the relaxation time with the droplet radius and the radius independent maximum velocity at the cross-over between stage 2 and 3. To the best of our knowledge, the simple exponential decay Eq. (15), and the expressions for the respective maximum velocity Eq. (14) and time constant Eq. (16) provide the first quantitative description of the evolving velocity of an active Janus droplet.

Contributions to self-sustained Marangoni stresses could also arise from the dissolution of ethanol into the ambient oil phase. The relative magnitude of Marganoni stresses created by concentrations gradients of monoolein in the ambient phase and of ethanol in the droplet phase could not be quantified in the present experiments and even with unreported techniques (like Raman spectroscopy). Our unreported attempts to determine concentration gradients of ethanol or monoolein in the surrounding phase by CARS-microscopy failed due to a massive background caused by the squalane that is masking the signal for all relevant concentrations. Trying to determine concentration gradients inside water-rich droplets might be slightly easier from that perspective but suffers additionally from the optical interface provided by the squalane-water interface. However, although the concentration gradients could not be determined quantitatively, monoolein appears, qualitatively, to be the dominant source for the droplet propulsion.

Conflicts of interest

There are no conflicts to declare.

Acknowledgements

M.L., M.B., and R.S. acknowledges funding from SPP1726. We thank Eric Freier (Leibniz Institut für Analytische Wissenschaften -ISAS- e.V.) for generous help with CARS microscopy.

Notes and references

1 M. Schmitt and H. Stark, *Eur. Phys. Lett., 2013*, **101**, 44008
2 E. Lauga and T. R. Powers, *Rep. Prog. Phys., 2009*, **72**, 096601.
3 C. Bechinger, R. Di Leonardo, L. Harmut, C. Reichhardt, G. Volpe and G. Volpe *Rep. Mod. Phys., 2016*, **88**, 045006.
4 C. A. Whitfield and R. J. Hawkins, *New J. Phys., 2016* , **18** 123016.
5 M. Schmitt and H. Stark, *Phys. Fluids, 2016*, **28**, 012106.
6 M. Downton and H. Stark, *J Phys Condens Matter., 2009*, **21**, 20, 204101.
7 S. Yabunaka, T. Ohta and N. Yoshinaga, *J. Chem. Phys., 2012*, **136**, 074904.
8 K. John, M. Bär and U. Thiele, *Eur. Phys. J. E, 2005*, **18**, 183–199.
9 E. Tjhung, D. Marenduzzo and M. E. Cates, *Proc. Natl. Acad. Sci. U.S.A., 2012*, **109**, 12381.
10 K. Furtado, C. M. Pooley and J. M. Yeomans, *Phys. Rev. E, 2008*, **78**, 046308.
11 R. Seemann, J.–B. Fleury and C. Maass, *Eur. Phys. J. Special Topics, 2016*, **225**, 2227–2240.
12 S. Thutupalli, R. Seemann and S. Herminghaus, *New. J. Phys., 2011* , **13**, 073021.
13 K. Peddireddy, P. Kumar, S. Thutupalli, S. Herminghaus and C. Bahr *Langmuir, 2012*, **28**, 34, 12426–12431.
14 Z. Izri, M. N. van der Linden, S. Michelin and O. Dauchot *Phys. Rev. Lett., 2014*, **113**, 24, 248302.
15 M. Li, M. Brinkmann, I. Pagonabarraga, R. Seemann and J.–B. Fleury *Communications Physics, 2018*, **1**, 23.
16 H. Tanaka and T. Araki, *Phys. Rev. Lett., 1998*, **81**, 389–392.
17 F. Califano, R. Mauri, R. Shinnar, *Phys. Fluids, 2005*, **17**, 094109.
18 E. Bormashenko, Y. Bormashenko, R. Pogreb and O. Gendelman *Langmuir, 2011*, **27**, 7–10
19 J. Jeong, A. Gross, W. S. Wei, F. Tu, D. Lee, P. J. Collings, A. G. Yodh *Soft Matter, 2015*, **11**, 6747–6754.
20 C. H. Choi, D. A. Weitz and C.–S. Lee, *Advance Material, 2013*, **25**, 2536-2541.
21 J. Guzowski, P. M. Korczyk, S. Jakielaa and P. Garstecki, *Soft Matter, 2012* **8**, 7269-7278.
22 L. Wenxiu, H. Dong, G. Tang, T. Ma and X. Cao, *RSC Adv., 2015*, **5**, 23181.
23 Sagiv, J. *J. Am. Chem. Soc., 1980*, **102** 92–98.
24 M. Lessel et al., *Surf. Int. Anal., 2015*, **47**, 557-564.
25 Levich, V. G. Physicochemical Hydrodynamics (Prentice-Hall, Englewood Cliffs, NJ, 1962).
26 R. Efrat, A. Aserin, E. Kesselman, D. Danino, E. J. Wachtel and N. Garti, *Colloids and Surfaces A: Physicochem. Eng. Aspects, 2007* **299**, 133–145.
27 P. T. Spicer, K. L. Hayden, M. L. Lynch, A. Ofori-Boateng and J. L. Burns, *Langmuir, 2001*, **17**, 5748.
28 S. Engstrom, K. Alfons, M. Rasmusson and H. Ljusberg-Wahren, *Progr Colloid Polym Sci, 1998* **108**, 93–98.
29 M. J. Lighthill, *Communications on Pure and Applied Mathematics, 1952*, **2**, 109–118.
30 J. R. Blake, *Journal of Fluid Mechanics, 1971*, **46**, 199–???.
31 See supporting information at [URL will be inserted by publisher].
32 A.Y. Rednikov, Y.S. Ryazantsev, and M.G. Velarde *Physics of Fluids, 1994*, **6**, 451-468.
33 C. Maass, C. Kruger, S. Herminghaus and C. Bahr, *Annu. Rev. Condens. Matter Phys., 2016*, **7**, 6.1-6.23.